Extracting spatial–temporal coherent patterns in geomagnetic secular variation using dynamic mode decomposition

Rodrigo Chi-Durán[1], and Bruce A. Buffett[1]

[1]Department of Earth and Planetary Science, University of California, Berkeley, Berkeley, CA, 94720, USA

Key Points:

- Dynamic mode decomposition (DMD) is applied to the geomagnetic radial field and its time variation.
- Waves with 20-yr and 60-yr periods are identified from the DMD decomposition.
- The 60-yr waves are compatible with fluid stratification at the top of the core.

Corresponding author: Rodrigo Chi-Durán, rodrigo.chi@berkeley.edu

Abstract

Rapid growth of magnetic-field observations through SWARM and other satellite missions motivate new approaches to analyze it. Dynamic mode decomposition (DMD) is a method to recover spatially coherent motion with a periodic time dependence. We use this method to simultaneously analyze the geomagnetic radial field and its secular variation from CHAOS-7 at high latitudes. A total of five modes are permitted by noise levels in the observations. One mode represents a slowly evolving background state, whereas the other four modes describe a pair of waves; each wave is comprised of a complex DMD mode and its complex conjugate. The waves have periods of $T_1 = 19.1$ and $T_2 = 58.4$ years and quality factors of $Q_1 = 11.0$ and $Q_2 = 4.6$, respectively. A 60-year wave is consistent with previous predictions for zonal waves in a stratified fluid. The 20-yr wave is also consistent with previous reports at high latitudes, although its nature is less clear.

Plain Language Summary

New insights into the structure and dynamics of Earth's outer core are enabled by the acquisition of large quantities of magnetic field data from recent satellites missions. We exploit this growing dataset using a method called dynamic mode decomposition (DMD) and apply it for the first time to geomagnetic field observations. The DMD method identifies coherent spatial and temporal patterns in the observations, which can be used to identify waves. Two pairs of waves with nominal periods of 20 and 60 years are recovered from the CHAOS-7 model. The 60-year waves are compatible with fluid stratification at the top of the core. The second 20-year waves have been reported in previous studies, but their spatial structure appears to require a different interpretation. The DMD method is successful in identifying waves in noisy data and provides an important tool for analyzing time variations in the geomagnetic field.

1 Introduction

Observations of the geomagnetic field offer a wealth of information about the dynamics of Earth's deep interior. Historical records from the past 400 years (Jackson et al., 2000) are commonly used to construct models of the geomagnetic field and its first time derivative, often called secular variation. A large part of the secular variation is attributed to large-scale fluid motion near the surface of Earth's core (e.g. Holme et al. (2015)). Other contributions include magnetic diffusion and the effects of unresolved small-scale flow. Recent efforts to account for these effects (Gillet et al., 2019) rely on geodynamo simulations to establish statistical correlations between the predicted flow and the magnetic field. While this approach represents the forefront of current research, it does mean that our ability to recover dynamics from magnetic-field observations is dependent on prior assumptions about the nature of flow. A complementary approach relies on modern data-driven methods to identify and characterize patterns of change in the observations. One particular technique, known as *dynamic mode decomposition* (Schmid, 2022), is particularly well-suited to the analysis of magnetic-field observations because it allow us to establish modes (waves) in the data before attaching a physical interpretation. There is no requirement for each mode to have a common physical basis or interpretation, although we do expect a common set of background conditions. A primary motivation for this study is to explore the feasibility of using new data-driven approaches to assess the geomagnetic field.

Several factors prompt our interest in data-driven approaches. One is the availability of magnetic observations from satellite missions (e.g. *Orsted, CHAMP, SWARM*), which substantially improve the quality and quantity of information. Satellite-based observations give better spatial coverage and allow greater discrimination between the internal and external sources of the geomagnetic field compared to ground-based measurements (Friis-Christensen et al., 2006). This improvement in observations has occurred in parallel with advances in the methods used to construct geomagnetic field models. Weaker temporal regularization and more flexible descriptions of the time dependence (Olsen et al., 2006; Gillet et al., 2013; Finlay et al., 2016; Barrois et al., 2018) have enabled reliable estimates of the second time derivative of the geomagnetic field (known as secular acceleration). This information creates new opportunities for exploring the dynamics of Earth's core on timescales that are surprisingly short. Short pulses of secular acceleration have been detected in the equatorial region (Chulliat et al., 2010; Finlay et al., 2016) and at high latitudes below Alaska (Finlay et al., 2020; Chi-Durán et al., 2020). The duration of these events is sometimes only a few years, and the equatorial disturbances often coincide with magnetic jerks (Chulliat & Maus, 2014).

Observations of secular acceleration point to much richer dynamics on short timescales (Finlay et al., 2020). The origin of these fluctuations is not well understood, although several lines of evidence from geodynamo models point to hydromagnetic waves in the core (Aubert & Gillet, 2021). Additional evidence comes from models of secular acceleration (Chi-Durán et al., 2020). A snapshot of secular acceleration from the CHAOS-7 model (Finlay et al., 2016) in 2008.5 shows regions of high activity near the equator and at high latitudes (see Fig. S1 in the supplementary material). Disturbances propagate at velocities of several hundred km/yr, which is more than an order of magnitude faster than the largest fluid velocities inferred from secular variation. Waves are a viable interpretation of these rapid disturbances, and the DMD methodology is an ideal detection tool because it identifies spatially coherent structures with a periodic time dependence (see Section 2).

2 Dynamic Mode Decomposition

Dynamic mode decomposition (DMD) is a method to recover the dynamics of a physical system from observations (Schmid, 2010). It was originally devised for linear systems in the context of fluid mechanics (Schmid, 2011), although recent theoretical developments have paved the way for extensions to nonlinear systems (Rowley et al., 2009). To illustrate the fundamental concept we consider a linear system

$$\frac{d\mathbf{f}}{dt} = \mathbf{A}\mathbf{f} \tag{1}$$

for the time dependence of a vector $\mathbf{f}(t)$. Here $\mathbf{A}$ is a constant matrix and the elements of $\mathbf{f}$ might represent the values of a function on a spatial grid x_i ($i = 1, \ldots, n$). A general solution for an arbitrary time increment Δt is

$$\mathbf{f}(t_0 + \Delta t) = e^{\mathbf{A}\Delta t}\mathbf{f}(t_0) \equiv \tilde{\mathbf{A}}\,\mathbf{f}(t_0) \tag{2}$$

where $\mathbf{f}(t_0)$ denotes the initial condition at $t = t_0$. The goal of the DMD method is to recover an estimate for the finite-time matrix $\tilde{\mathbf{A}}$ using pairs of snapshots of the system. We define a data matrix

$$\mathbf{F} = [\mathbf{f}(t_0)\ \mathbf{f}(t_1)\ ..., \mathbf{f}(t_{m-1})] \tag{3}$$

and let

$$\mathbf{F}' = [\mathbf{f}(t_1)\ \mathbf{f}(t_2)\ ..., \mathbf{f}(t_m)] \tag{4}$$

be the data matrix at a subsequent snapshot (e.g.. $t_k = t_{k-1} + \Delta t$). An optimal approximation for $\tilde{\mathbf{A}}$ minimizes the misfit to

$$\mathbf{F}' = \tilde{\mathbf{A}}\mathbf{F}\,. \tag{5}$$

Once we establish the matrix operator $\tilde{\mathbf{A}}$ from Eq. 5, we can evolve the system forward in time using

$$\mathbf{f}(t_k) = \tilde{\mathbf{A}}\mathbf{f}(t_{k-1})\,. \tag{6}$$

Several implementations of the DMD method have been proposed (e.g. Brunton and Kutz (2019); Schmid (2022)). We follow the approach called exact DMD (Tu et al., 2014), which differs slightly in the way the eigenvectors of $\tilde{A}$ are computed. The eigenvalues and eigenvectors of $\tilde{\mathbf{A}}$ define the dynamic modes, although in practice the modes are computed by first projecting $\tilde{\mathbf{A}}$ onto the leading principal components (singular vectors) of the data matrix $\mathbf{F}$. In effect, we use coherent spatial structure from the data matrix to construct $\tilde{\mathbf{A}}$ (see Tu et al. (2014) for details). When r singular values are retained in the singular value decomposition of $\mathbf{F}$, the reconstruction of the data can be written as

$$\mathbf{f}(t_k) = \sum_{j=1}^{r} \mathbf{\Phi}_j [\tilde{\lambda}_j]^k b_j \tag{7}$$

where $\mathbf{\Phi}_j$ is the eigenvector and $\tilde{\lambda}_j$ is the eigenvalue of $\tilde{\mathbf{A}}$, which has been raised to the kth power in Eq. 7; b_j defines the mode amplitude, such that the initial condition can be written as a linear combination of the modes

$$\mathbf{f}(t_0) = \sum_{j=1}^{r} \mathbf{\Phi}_j b_j \, . \tag{8}$$

We can express Eq. 7 in a more convenient form by noting that the eigenvalues of $\tilde{\mathbf{A}}$ are related to the eigenvalues λ_j of the original $\mathbf{A}$ matrix in Eq. 1 (e.g., Perko (2013)). Letting

$$\tilde{\lambda}_j = \exp(\lambda_j \Delta t) \tag{9}$$

allows us to rewrite the data reconstruction as

$$\mathbf{f}(t_k) = \sum_{j=1}^{r} \mathbf{\Phi}_j [e^{\lambda_j k \Delta t}] b_j \tag{10}$$

where we see that the time dependence of the system is explicitly recovered through the DMD procedure. We can think of the DMD modes a linear combination of principal components (or EOFs) that evolve with a complex frequency λ. This makes DMD ideal for detecting waves in magnetic-field models because any coherent wave structure is expected to have a specific frequency. In general the frequencies will be complex (i.e. $\lambda = \sigma_j + i\omega$) so we can define the quality factor (Q) of a mode as

$$Q_j = \frac{\omega_j}{2\sigma_j} \, . \tag{11}$$

Finally, it is important to note that complex eigenvalues appear as complex conjugate pairs when the input data is real; if λ is a complex eigenvalue of $\mathbf{A}$ then the complex conjugate λ^* is also a eigenvalue of $\mathbf{A}$. This means that a pair of DMD modes have the same frequency ω.

3 Results

We model the geomagnetic radial field and secular variation simultaneously by defining a state vector as (see Eq. 1)

$$\mathbf{f} = \begin{bmatrix} \mathbf{B_r} \\ \dot{\mathbf{B}}_\mathbf{r} \end{bmatrix} \tag{12}$$

where $\mathbf{B_r}$ and $\dot{\mathbf{B}}_\mathbf{r}$ are the geomagnetic radial field (in 10^{-9} [T]) and secular variation (in 10^{-10} [T/yr]), respectively from CHAOS-7.12 (Finlay et al., 2020). (The choice of units is intended to give slightly higher weight to the time rate of change of secular variation in the construction of the system matrix A.) The augmented state vector means that our linear system in Eq. 1 corresponds to the coupled equations for secular variation and secular acceleration. The state vector is evaluated between 1998 and 2019 using a geographic grid with 100 grid points in latitude and 200 grid points in longitude. We restrict the DMD analysis to the Northern Hemisphere between latitudes 30°N and 90°N. The number of modes used in the calculation is set by the level of coherence in the observations (see next Section). We use 5 singular values in the construction of the DMD modes to produce 5 modes. The first mode describes a secular trend with an infinite period (zero frequency). We interpret this mode as the slowly evolving structure of the main field and secular variation. The other four modes represent two waves with periods of 19.1 and 58.4 years and quality factors of 11.0 and 4.6, respectively. The spatial structure of the four wave-like modes is shown in Fig. 1. The corresponding time dependence of each modes is shown in Fig. 2. These specific predictions are obtained when the CHAOS-7 model is truncated at degree $\ell = 14$. Small changes in the periods are found when the truncation is increased, whereas the spatial structures of the modes are nearly invariant.

A superposition of the first 5 DMD modes accurately reconstructs the original signal from CHAOS-7 (Fig. 3a). For example, Mode 1 in Fig. 3b gives a reasonable description of the main field. Adding Modes 2 and 3 to Mode 1 captures most of the variability in CHAOS-7 (compare Fig. 3a and Fig. 3c). Adding Modes 4 and 5 (see Fig. 3d) produces only small changes in the reconstruction. We conclude that the first five modes are sufficient to recover most of the original signal.

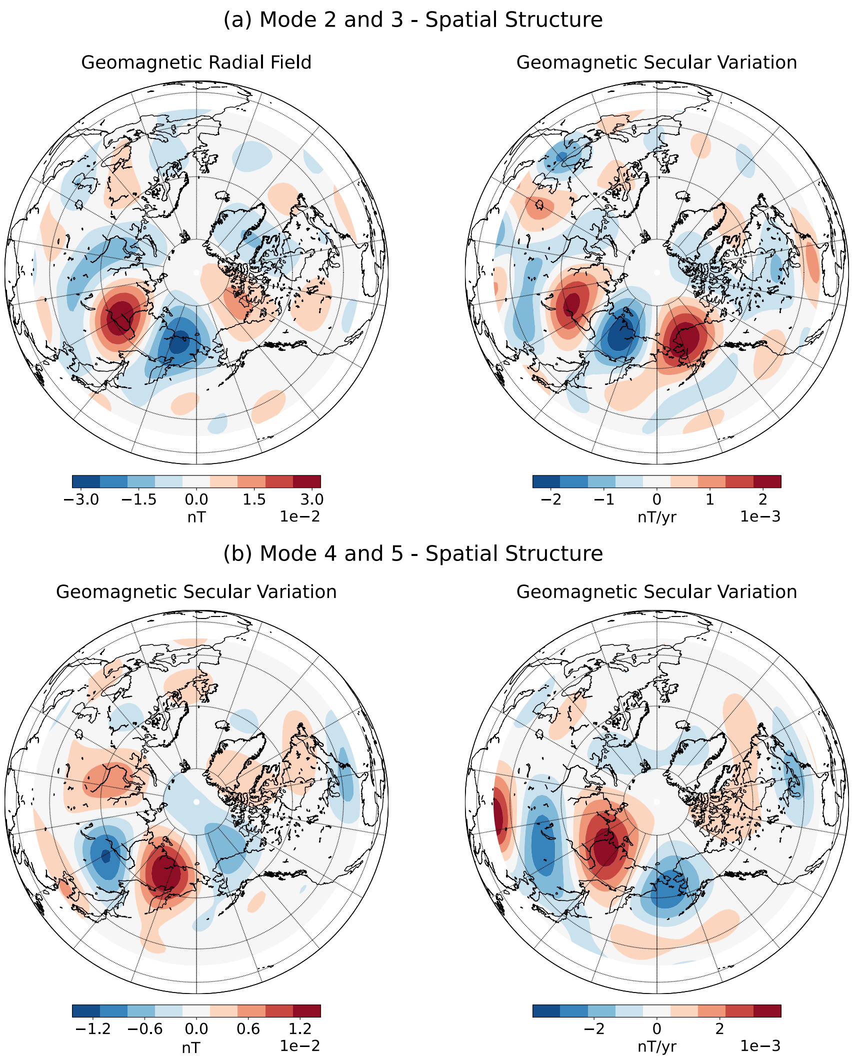

Figure 1. (a) Spatial structure of the Modes 2 and 3 with a period of 58.4 years. (b) Spatial structure of the Modes 4 and 5 with a period of 19.2 years. To reconstruct the magnetic field and secular variation at a given time, it is necessary to multiply the modes by their amplitudes b_i and by their temporal dependence (see Figure 2).

4 Discussion

Application of the DMD methodology to the Northern Hemisphere reveals three distinct types of variability in the geomagnetic field. We detect a slow secular trend and two damped waves. The fact that distinct wave features are recovered by the DMD method means that we are finding coherent spatial and temporal structure in the CHAOS-7 model. We now turn to the question of whether we can identify the origin of this coherent structure.

Mode 1 represents a steady trend in the geomagnetic field. The amplitude of the recovered mode increases linearly at a rate of about 0.3% per year (see Figure 2a). The eigenvalue of Mode 1 is purely real, which means that ω vanishes and the period $2\pi/\omega$ is infinite. This mode accounts for the spatial structure of the geomagnetic radial field and its slow secular trend. Deviations from this secular trend are described by the other DMD modes.

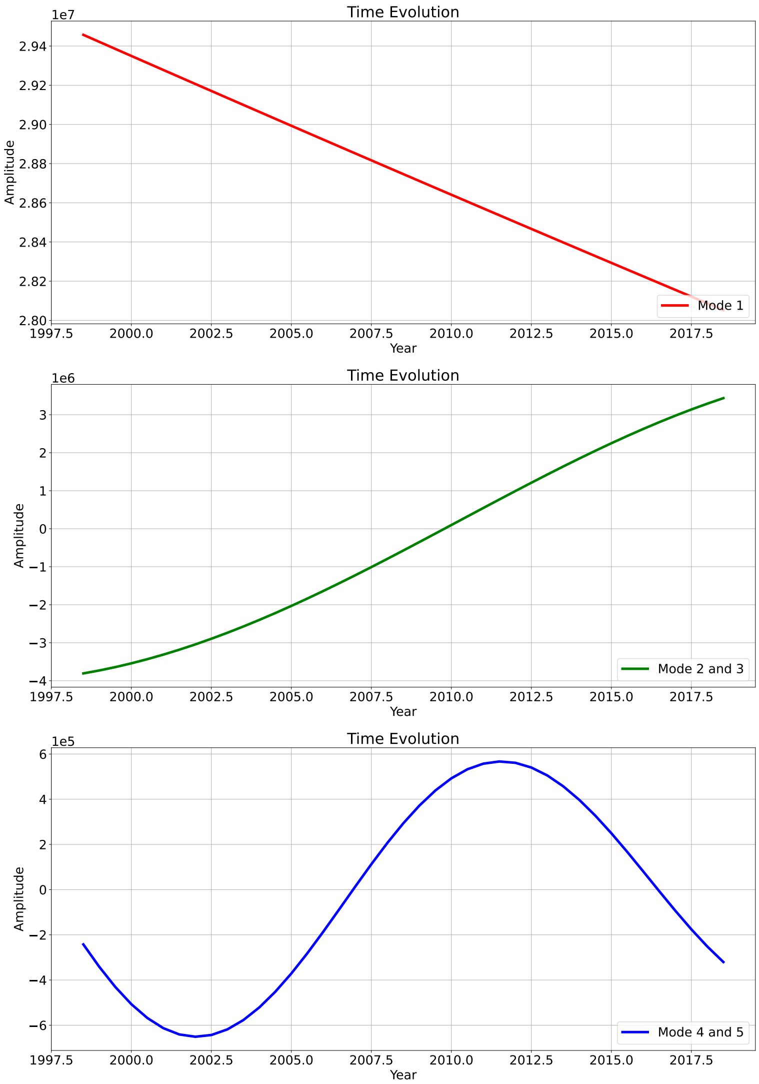

Figure 2. (a) Temporal evolution of Mode 1. This mode represents a secular trend with an infinite period. (b) Temporal evolution of Modes 2 and 3 corresponds to a period of 58.4 years and quality factor of 4.6. (c) Temporal evolution of Modes 4 and 5 corresponds a period of 19.1 years and quality factor of 11.0.

The oscillatory modes are needed to reconstruct short-period variations in the original signal. The most prominent feature in B_r and $\dot{B}_r$ is due to a mode with a nominal 60-year period. Figure 4 shows the average misfit between the reconstruction and CHAOS-7 using a different combination of modes. The average misfit is calculated as the average of absolute value of the difference between the reconstruction of the signal (superposition of modes) and the original data. The total misfit is divided by the number of grid points in the sum. Reconstructions that do not include the 60-year variation in Modes 2 and 3 have a higher misfit in both the radial magnetic field and the secular variation. By comparison, Modes 4 and 5 contribute much less to the variation. This can be seen by comparing the misfit for Modes 1, 2 and 3 with that for Modes 1, 4 and 5 (see Fig. 4). The first combination (Modes 1,2, and 3) lowers the average misfit by approximately one of magnitude relative to the second combination (Modes 1, 4, and 5). On the other hand, there is a discernible improvement in the misfit to B_r and $\dot{B}_r$ when all five modes

Figure 3. (a) Geomagnetic radial field and geomagnetic secular variation from CHAOS7. (b) Geomagnetic radial field and geomagnetic secular variation from Mode 1 (c) Geomagnetic radial field and geomagnetic secular variation using the superposition of modes 1, 2 and 3 (c) Geomagnetic radial field and geomagnetic secular variation using all modes (1, 2, 3, 4 and 5). All quantities are calculated at $t = 2005.5$ using $\ell = 14$ for the model truncation.

are included. The time average misfit using all five modes corresponds 0.1% in the geomagnetic radial field and 11% in the geomagnetic secular variation.

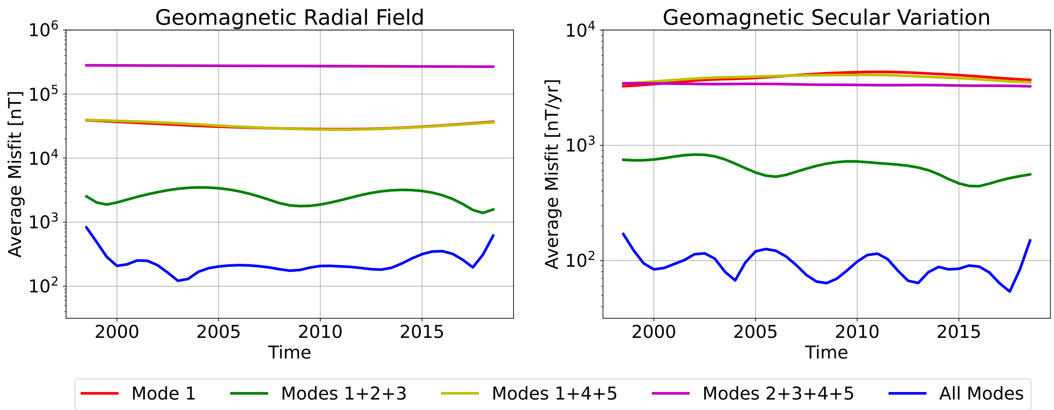

Figure 4. Misfit to the geomagnetic radial field and the geomagnetic secular variation over time when different modes are included in the reconstruction.

A nominal 60-year wave in the secular variation is broadly consistent with previous studies (Yokoyama & Yukutake, 1991; Roberts et al., 2007). One possible interpretation of the 60-year variation is due to a zonal MAC wave, which depends on the existence of stable stratification at the top of the core. Buffett et al. (2016) showed that a zonal MAC wave, identified by spherical harmonic degree $\ell = 4$, could account for fluctuations in both the geomagnetic field and the length of day. In this study we reproduce the predictions for an $\ell = 4$ MAC wave using a physical model that allows for latitudinal changes in the rms radial magnetic field (Buffett & Knezek, 2018). Here we let the mean-square radial field increase by a factor of 3.5 between the equator and the pole, consistent with predictions from dynamo models. The overall intensity of the radial field is defined to have an surface-averaged rms strength of 0.5 mT. Predictions with this choice of rms radial field provide a reasonable fit to the spatial structure of Modes 2 and 3 (only Mode 3 is shown in Figure 5. The most prominent features in Mode 3 are the alternating patches of secular variation below Siberia and Alaska. A similar pattern of secular variation is also evident in the predictions for the $\ell = 4$ MAC wave, although there are notable differences. In particular we find a strong negative patch in the secular variation below central Asia, which is much weaker in the DMD mode. There also appears to be a 20° shift in the longitude of the peak variations at high latitudes. Further differences below the Atlantic and Greenland also contribute to a surprisingly large $\mathcal{O}(1)$ misfit, despite the qualitative visual similarity of the two signals. Other MAC waves with higher ℓ have greater spatial complexity, which introduces features that are not seen in Mode 3.

Estimates for the period and damping of Mode 3 constrain the choice of physical properties for the wave model. Of particular interest is the thickness and strength of stable stratification at the top of the core. To be specific we allow a linear variation in buoyancy frequency N across the layer, starting with a value $N = 0$ at the base of the layer. In this case the layer properties are fully defined by the layer thickness and the peak buoyancy frequency at the core-mantle boundary. To illustrate we consider a 140-km thick layer with a peak buoyancy frequency of $N_{max} = 0.86\Omega$, where Ω is the Earth's rotation frequency. An $\ell = 4$ MAC wave has a period of 58.4 years and a quality factor $Q =$ 2.8, which is broadly compatible with the complex frequency of Modes 2 and 3. Weaker secular variation due to waves in the southern hemisphere is expected because the horizontal gradients in the radial field are smaller in this region.

Figure 5. Comparison of DMD mode 3 and with predictions for three zonal MAC waves, identified by the dominant spherical harmonic degree $\ell = 4$, $\ell = 6$ and $\ell = 8$. All comparisons are made at $t = 1998.5$.

The DMD method also identifies a nominal 20-year wave, which has been previously reported in the Northern Hemisphere (Chi-Durán et al., 2020; Chi-Durán et al., 2021). However, the origin of Modes 4 and 5 is less clear. It is reasonable to ask if the 20-year wave could be attributed to a zonal MAC wave with higher ℓ. To explore this possibility we adopt a 140-km layer with a peak buoyancy frequency of $N = 0.86\Omega$. Our prediction for $\ell = 12$ wave gives a period of 18.9 years and a quality factor of 4.6. While the period is in reasonable agreement, the quality factor is lower than $Q = 11.0$ for Modes 4 and 5. In addition, the spatial complexity of the predicted secular variation for an $\ell =$ 12 wave is not compatible with the structure of Modes 4 and 5. (Note that the spatial structure of the secular variation depends on the wave structure and the distribution of radial magnetic field). Predictions for an $\ell = 8$ wave in Fig. 5 are already too complicated compared to the spatial structure of Modes 4 and 5 in Fig. 1. Increasing the degree to $\ell = 12$ to match the period only makes the comparison of the spatial structure worse. We conclude that the predicted spatial patterns of higher ℓ MAC waves are not compatible with the spatial structure of Modes 4 and 5. Other types of waves should be explored to identify the origin of Modes 4 and 5. Alternatively, the geomagnetic signal may be a consequence of flow associated with the tangent cylinder (Livermore et al., 2017)

Our calculation of DMD modes depends on the number of singular values we use to construct the optimal dynamics matrix A. This choice determines the number of DMD modes that are recovered from the data. Since the DMD modes are not orthogonal we can expect a change in the spatial structure of the individual modes as the number of singular values are increased. Even though the overall fit to the observations should improve as the number singular values increases, our ability to interpret the individual modes could be compromised if these modes change when we retain too many singular values.

There are several ways to make an objective choice for the number of singular values. In this study we have followed the approach advocated by Brunton and Kutz (2019). This method sets a target for the cumulative variance (or energy) recovered from the original data by a limited number of singular values. In Fig. S2, we plot the cumulative variance as a function of the number of singular values. Setting the threshold at 99.5% of the total variance limits the reconstruction to the first 5 modes. Contributions from individual modes above this threshold do little to improve the fit to the data.

Finally, we comment on the recovery of DMD modes with periods that exceed the duration of the record. We recall that the DMD method finds the optimal dynamics matrix $\tilde{A}$. In principle, a long-period oscillation could be recovered from a short record if the underlying dynamics is linear. Practical limitations arise in the presence of noise or when the dynamics is nonlinear. One way to test the recovery of long-period modes is to repeat the analysis on a longer record. For example, we consider a 30-year record of radial magnetic field and secular variation between 1988 and 2018 from the COV-OBSx2 model (Huder et al., 2020). We confine our attention to the northern hemisphere (as before) and retrieve 6 DMD modes from the longer record. Two modes correspond to secular trends ($\omega = 0$). The other four modes correspond to a pair of waves with periods of 51 years and 19.6 years. The amplitude of the 51-year mode is slightly smaller than the corresponding 60-year mode recovered from CHAOS-7 but the spatial structure of the mode is remarkably similar to that from CHAOS-7 (see Figure S3).

Extending the COV-OBSx2 record to 55 years (1963 to 2018) has very little influence on the spatial structure of the 60-year DMD modes (see Figure S3), although the period increases to 74 years. While a longer record should improve the reliability of the recovered period, there is also a greater chance that stochastic generation of the wave by convection in the core will alter the temporal coherence. Broadly similar results from the shorter CHAOS-7 record is encouraging because we might try to average modes from short records to reduce the contribution of the generation process.

5 Conclusions

We apply the DMD technique to geomagnetic observations to quantify waves in the core. By combining observations of the geomagnetic field and secular variation we obtain an optimal description of the time variations in B_r and $\dot{B}_r$, corresponding to equations for secular variation and secular acceleration of the field. This is a powerful approach because no priori physical knowledge is needed to construct the modes. We simply look for patterns of spatial and temporal coherence in the observations. The DMD methodology opens a new way to study the time dependence of geomagnetic data and extract information about waves in the core.

The DMD modes recovered from the simultaneous analysis of B_r and $\dot{B}_r$ are compatible with the existence of two waves. One with a nominal period of 20 years and another with a nominal period of 60 years. Both of these waves had been reported in previous studies (Chi-Durán et al., 2020; Buffett et al., 2016). The advantage of the DMD method is that we recover estimates of the spatial structure and the frequency of the waves, including the damping time. The nominal 60-year wave is compatible with the structure and frequency of a zonal MAC wave, which requires fluid stratification at the top of the core. The shorter period wave does not appear to be due to a higher frequency (zonal) MAC wave. Other physical processes may contribute to origin of the 20-year variations.

Open Research

The source code and the DMD implementation are available online (Chi-Durán, 2022).

Acknowledgments

We thank Phil Livermore and an anonymous reviewer for constructive suggestions that improved the paper. We also thank Chris Finlay and Nicholas Gillet for help with the CHAOS-7 and COV-OBSx2 models. R.C.-D. acknowledges the support from the Fulbright Foreign Student Program and the National Agency for Research and Development (ANID) Scholarship Program/DOCTORADO BECAS CHILE/2015-56150003. This work is also partially supported by the National Science Foundation EAR-2214244 to B. B.

References

Aubert, J., & Gillet, N. (2021). The interplay of fast waves and slow convection in geodynamo simulations nearing Earth's core conditions. *Geophys. J. Int.*, *225*(3), 1854–1873. doi: https://doi.org/10.1093/gji/ggab054

Barrois, O., Hammer, M. D., Finlay, C. C., Martin, Y., & Gillet, N. (2018, October). Assimilation of ground and satellite magnetic measurements: inference of core surface magnetic and velocity field changes. *Geophys. J. Int.*, *215*(1), 695–712.

Brunton, S. L., & Kutz, J. N. (2019). *Data-driven science and engineering: Machine learning, dynamical systems, and control*. Cambridge University Press. doi: 10.1017/9781108380690

Buffett, B., & Knezek, N. (2018). Stochastic generation of MAC waves and implications for convection in earth's core. *Geophys. J. Int.*, *212*(3), 1523–1535. doi: https://doi.org/10.1093/gji/ggx492

Buffett, B., Knezek, N., & Holme, R. (2016). Evidence for MAC waves at the top of earth's core and implications for variations in length of day. *Geophys. J. Int.*, *204*(3), 1789–1800. doi: https://doi.org/10.1093/gji/ggv552

Chi-Durán, R., Avery, M. S., & Buffett, B. A. (2021, October). Signatures of high-latitude waves in observations of geomagnetic acceleration. *Geophys. Res. Lett.*.

Chi-Durán, R. (2022, December). *Dynamic mode decomposition code for Geomagnetic Radial Field and Secular Variation.* Zenodo. Retrieved from `https://doi.org/10.5281/zenodo.7450131` doi: 10.5281/zenodo.7450131

Chi-Durán, R., Avery, M. S., Knezek, N., & Buffett, B. A. (2020, September). Decomposition of geomagnetic secular acceleration into traveling waves using complex empirical orthogonal functions. *Geophys. Res. Lett.*, *47*(17), 1.

Chulliat, A., & Maus, S. (2014). Geomagnetic secular acceleration, jerks, and a localized standing wave at the core surface from 2000 to 2010. *J. Geophys. Res. [Solid Earth]*.

Chulliat, A., Thébault, E., & Hulot, G. (2010). Core field acceleration pulse as a common cause of the 2003 and 2007 geomagnetic jerks. *Geophys. Res. Lett.*, *37*(7). doi: https://doi.org/10.1029/2009GL042019

Finlay, C. C., Kloss, C., Olsen, N., Hammer, M. D., Tøffner-Clausen, L., Grayver, A., & Kuvshinov, A. (2020, October). The CHAOS-7 geomagnetic field model and observed changes in the south atlantic anomaly. *Earth Planets Space*, *72*(1), 156.

Finlay, C. C., Olsen, N., Kotsiaros, S., Gillet, N., & Tøffner-Clausen, L. (2016, July). Recent geomagnetic secular variation from swarm and ground observatories as estimated in the CHAOS-6 geomagnetic field model. *Earth Planets Space*, *68*(1), 112.

Friis-Christensen, E., Lühr, H., & Hulot, G. (2006, April). Swarm: A constellation to study the earth's magnetic field. *Earth Planets Space*, *58*(4), 351–358.

Gillet, N., Huder, L., & Aubert, J. (2019, October). A reduced stochastic model of core surface dynamics based on geodynamo simulations. *Geophys. J. Int.*, *219*(1), 522–539.

Gillet, N., Jault, D., Finlay, C. C., & Olsen, N. (2013, April). Stochastic modeling of the earth's magnetic field: Inversion for covariances over the observatory era. *Geochem. Geophys. Geosyst.*, *14*(4), 766–786.

Holme, Olson, & Schubert. (2015). Large-scale flow in the core. *Treatise on geophysics*.

Huder, L., Gillet, N., Finlay, C. C., Hammer, M. D., & Tchoungui, H. (2020). COV-OBS.x2: 180 years of geomagnetic field evolution from ground-based and satellite observations. *Earth, Planets, Space*, *72*, 160. doi: https://doi.org/10.1186/s40623-020-01194-2

Jackson, A., Jonkers, A. R. T., & Walker, M. R. (2000, March). Four centuries of geomagnetic secular variation from historical records. *Philosophical Transactions of the Royal Society of London. Series A: Mathematical, Physical and Engineering Sciences*, *358*(1768), 957–990.

Livermore, P. W., Hollerbach, R., & Finlay, C. C. (2017). An accelerating high-latitude jet in Earth's core. *Nat. Geosci.*, *10*, 62-68. doi: https://doi.org/10

.1038/ngeo2859
Olsen, N., Lühr, H., Sabaka, T. J., Mandea, M., Rother, M., Tøffner-Clausen, L., & Choi, S. (2006, July). CHAOS—a model of the earth's magnetic field derived from CHAMP, ørsted, and SAC-C magnetic satellite data. *Geophys. J. Int.*, *166*(1), 67–75.
Perko, L. (2013). *Differential equations and dynamical systems.* Springer Science & Business Media.
Roberts, P. H., Yu, Z. J., & Russell, C. T. (2007). On the 60-year signal from the core. *Geophys. Astrophys. Fluid Dyn.*, *101*, 11-35. doi: https://doi.org/10.1080/03091920601083820
Rowley, C. W., Mezić, I., Bagheri, S., Schlatter, P., & Henningson, D. S. (2009, December). Spectral analysis of nonlinear flows. *J. Fluid Mech.*, *641*, 115–127.
Schmid, P. J. (2010). Dynamic mode decomposition of numerical and experimental data. *Journal of Fluid Mechanics*, *656*, 5–28. doi: 10.1017/S0022112010001217
Schmid, P. J. (2011, April). Application of the dynamic mode decomposition to experimental data. *Exp. Fluids*, *50*(4), 1123–1130.
Schmid, P. J. (2022, January). Dynamic mode decomposition and its variants. *Annu. Rev. Fluid Mech.*, *54*(1), 225–254.
Tu, J. H., Rowley, C. W., Luchtenburg, D. M., Brunton, S. L., & Nathan Kutz, J. (2014, December). On dynamic mode decomposition: Theory and applications. *Journal of Computational Dynamics*, *1*(2), 391–421.
Yokoyama, Y., & Yukutake, T. (1991). Sixty year variation in a time series of geomagnetic gauss coefficients between 1910 and 1983. *J. Geomagn. Geoelect.*, *43*, 563-584. doi: https://doi.org/10.5636/jgg.43.563